Thermal and Crystallisation Kinetics of Yttrium-Doped Phosphate-Based Glasses

Abul Arafat[1], Sabrin A. Samad[1], Matthew. D. Wadge[1], Md Towhidul Islam[1], Andrew. L. Lewis[2], Emma R. Barney[1] and Ifty Ahmed[1]

[1]Faculty of Engineering, Advanced Materials Research Group, University of Nottingham, Nottingham, UK

[2]Biocompatibles UK Ltd., a BTG International group company, Lakeview, Riverside Way, Watchmoor Park, Camberley, Surrey, GU15 3YL, UK

Correspondence: Ifty Ahmed, Email:ifty.ahmed@nottingham.ac.uk

Abstract

Yttrium doped glasses have been utilised for biomedical applications such as radiotherapy especially for liver cancer treatment. In this paper, the crystallisation behaviour of phosphate-based glasses doped with yttrium (in the system $45P_2O_5$-(30-x) Na_2O-25CaO-xY_2O_3 – where x= 0, 1, 3 and 5) have been investigated via Differential Scanning Calorimetry (DSC) using non-isothermal technique at different heating rates (5°C, 10°C, 15°C and 20°C/min). The glass compositions were characterised via EDX, XRD, Density and Molar volume analysis. The Moynihan and Kissinger methods were used for the determination of glass transition activation energy (E_g) which decreased from 192 kJ/mol to 118 kJ/mol (Moynihan) and 183 kJ/mol to 113 kJ/mol (Kissinger) with increasing yttrium oxide content. Incorporation of 0 to 5 mol% Y_2O_3 revealed an approximate decrease of 71 kJ/mol (Ozawa and Augis) for onset crystallisation (E_x) and 26 kJ/mol (Kissinger) for crystallisation peak activation energies (E_c). Avrami index (n) value analysed via Matusita-Sakka equation suggested a one-dimensional crystal growth for the glasses investigated. SEM analysis explored the crystalline morphologies and revealed one-dimensional needle-like crystals. Overall, it was found that

these glass formulations remained amorphous with up to 5 mol% Y_2O_3 addition with further increases in Y_2O_3 content resulting in significant crystallisation.

Keywords: Yttrium phosphate glass, DSC, Crystallisation kinetics, Crystal growth

1. Introduction:

Phosphate-based glasses have been widely investigated for biomedical applications and can provide highly useful properties such as low glass transition and melting temperatures, high thermal expansion coefficients, biocompatibility, high refractive indices and one of their most unique offerings is their controlled dissolution properties. (1). The structural, chemical and physical durability of phosphate glasses has been shown to be improved by the inclusion of several oxide additions such as ZnO (2,3), Fe_2O_3 (4,5), Y_2O_3 (6,7), Al_2O_3 (8,9), TiO_2 (10,11) and Bi_2O_3 (12,13).

Amongst these, yttrium oxide containing glasses are an area of interest due to their characteristic structural and physical properties such as high refractive index, high thermal expansion coefficient, density and excellent infrared transmission (14). Moreover, it has also demonstrated highly useful application in radiotherapy (15–17) due to the relatively short half-life and beta emission properties of the ^{90}Y isotope (18–20).

Y_2O_3 plays a vital role in improving the properties of glasses. Within glass systems, yttrium oxide can act as a network modifier or as a network former depending on glass composition and the amount of Y_2O_3 within the glass (14,21,22). Singh *et al.* investigated the 55 SiO_2–30 B_2O_3–x Li_2O–(15-x) Y_2O_3 glass system and reported that Y_2O_3 changed its role from glass former to network modifier as its concentration exceeded 5 mol% (14). Furthermore, incorporation of Y_2O_3 into the zinc borosilicate glass system was reported to increase glass stability by 20°C with increasing yttria content from 0 to 3 mol% (23). Mahdy *et al.* investigated yttrium aluminosilicate glasses and stated that the glass stability increased due to replacing Al_2O_3 with Y_2O_3 resulting in greater strength of the cross-links between the Y^{3+} cation and oxygen atoms, leading to an increase in the structural rigidity of the glasses (22).

This increase in stability can be related to the crystallisation kinetics and activation energy of the glass systems (24) which also correlates with the crystallisation behaviour of the glasses. The higher the activation energy, the less prone the glass will be to crystallise (25).

Crystallisation kinetics of yttrium silicate glasses have been reported in the literature (26–29). Wang *et al.* studied yttrium zinc borosilicate glasses and stated that addition of Y_2O_3 enhanced the glass thermal stability and addition of more than 8 mol% of Y_2O_3 revealed that the glass began to crystallise due to tendency of supersaturation in the glassy state (30). Vishal *et al*. studied the crystallisation behaviour of a yttrium and lanthanum calcium borosilicate glass to explore the suitability of this glass as a sealant and they found that this glass was a good candidate as compared to yttrium calcium borosilicate glass due to higher thermal expansion coefficient, low fragility index value and viscosity profile (26). Studies on crystallisation kinetics of lithium (31), copper (32), calcium (33) and aluminium (9) phosphate glasses have been reported. Limited studies have been reported on the crystallisation behaviour of yttrium phosphate glasses. Petra *et al.* studied on crystallisation kinetics of erbium doped yttrium phosphate glasses based on particle size of the powder and bulk sample (34).

In order to explore crystallisation kinetics and thermal stability of glasses, differential thermal analysis (DTA) and differential scanning calorimetry (DSC) are popular methods for studying the kinetics of non-isothermal data (35,36). These methods are relatively straight-forward to carry out, requiring only small sample volumes and possessing flexibility in the ability to vary the heating rates. Between these two techniques, DSC is widely used due to its simplicity and sensitivity (37,38). Isothermal and non-isothermal methods are the two basic methods in DSC analysis. For the isothermal method, the sample is heated up to a temperature above glass transition (T_g) and the heat evolution during the crystallisation process is recorded as a

function of time where the temperature is kept constant. For non-isothermal analysis, the sample is heated at a fixed rate and the heat evolved is recorded as a function of temperature and time (39) and is more widely used due to its simplicity and rapid method (40,41).

In the present investigation, the glass transition temperature and crystallisation kinetics were studied as a function of the Y_2O_3 content in phosphate glasses using non-isothermal DSC analysis. The Moynihan (42), Kissinger (43), Ozawa (44), Augis-Bennette (45) and Matusita–Sakka (46) equations were used for the determination of crystallisation kinetics and activation energies for glass transition, onset crystallisation and crystallisation temperature.

2. Materials and Methods:

2.1 Glass synthesis:

Four different glass compositions were prepared using sodium dihydrogen phosphate (NaH_2PO_4), calcium hydrogen phosphate ($CaHPO_4$), yttrium oxide (Y_2O_3) and phosphorous pentoxide (P_2O_5) (Sigma Aldrich, UK) as starting materials. The precursors were mixed together and transferred to a 10%Rh/Pt crucible (Birmingham Metal Company, UK) which was placed in a furnace preheated to 350°C for half an hour and 500°C for an hour depending on the glass compositions for the removal of H_2O. The mixtures were then heated at 1150°C for the yttrium free glass and 1300°C for the yttrium containing glasses, for 2 hours as shown in Table 1. The resultant melts were poured onto a steel plate and left to cool to room temperature. The glass was then crushed using a planetary ball mill (Retsch PM100) and sieved to obtain a glass particle size range of between 25-45 µm.

2.2 Powder X-ray diffraction analysis:

The as-quenched glass was used for XRD analysis to investigate the amorphous nature of the glass compositions produced. The data was collected on a Bruker AXS–D8 Advance powder diffractometer in flat plate geometry using Ni-filtered Cu-Kα radiation (λ=0.15418 nm), operated at 40kV and 35mA. The angular range 2θ for each scan was from 10° to 70° with a step size of 0.1° and a step time of 5s. The phases were identified using the EVA software *via* Crystallographic Search-Match icon (DIFFRACplus Suite,Bruker-AXS) and the International Centre for Diffraction Data (2005).

2.3 Energy dispersive X-ray analysis:

Portions of the glass samples from each composition were polished using SiC paper and diamond cloths with industrial methylated spirit (IMS) as eluent. The samples were then dried and cleaned by air dry spray before being carbon coated. Energy dispersive x-ray (EDX) analysis was performed on an EDAX model DX 4 using ZAF quantitative analysis. The accelerating voltage was maintained at 15 kV and the system resolution was 60 eV with a live time of 120 seconds. Jadeite (for Na), gallium phosphide (for P), wollastonite (for Ca) and yttrium (for Y) were used as a standard for analysis. The working distance was 10 mm and the EDX spectrometer was connected to the Philips XL30 SEM. An average of five separate areas were analysed for the final composition of the materials.

2.4 Helium pycnometry:

Density measurements were conducted using a Micromeritics AccuPyc 1330 helium pycnometer (Norcross, GA, USA). 'Archimedes' principle of fluid displacement was employed to determine the volume of the solid objects. Calibration of the equipment was conducted using a standard calibration ball (3.18551 cm^3) with errors of ±0·05%. Approximately 3.5 g of the samples were used for measurement and the process was repeated three times. For each formulation the molar volume was calculated using the equation 1:

$$V_m = \frac{\sum_i xiMi}{\rho} \quad (1)$$

where x_i is the molar fraction of the *i*th component, ρ is the density, and M_i is the molecular weight of the *i*th component.

2.5 Thermal analysis:

Approximately 10 mg samples of the glass powders (size range of 25 and 45 µm) were tested to determine the thermal properties such as glass transition (T_g), onset of crystallisation (T_x), crystallisation (T_c) and melting (T_m) temperature using a simultaneous thermal analysis (TA Instruments SDT Q600, USA). Glass particles were placed into a platinum pan and heated from room temperature to 1100°C at different heating rates (i.e. 5, 10, 15 and 20°C/min) under argon gas flow (50 ml/min). A blank run was carried out to determine the baseline which was then subtracted from the plot obtained using TA universal analysis 2000 software. The thermal stability of the glasses was measured in terms of the processing window by taking the temperature difference between the glass transition temperature (T_g) and the onset of crystallisation temperature (T_x) as shown in the following:

$$\text{Processing window} = T_x - T_g \quad (2)$$

2.6 SEM analysis:

For imaging analysis, a JEOL 7100F Field-Emission Gun Scanning Electron Microscope (FEG-SEM) and scanning electron microscope (SEM, Phillips FEI XL30, USA) utilising a 15 kV beam set at a working distance of 10 mm, were used to investigate the glass formulations produced and the samples which crystallised. Prior to acquisition, the samples were mounted in an epoxy resin block, which were ground using varying grits (P240-P1200), followed by polishing on 6 and 1 µm diamond polishing pads respectively. The polished blocks were then eroded in 4 % (mass concentration) HF for 20 s each. The etched samples were subsequently cleaned with deionised water and air dried. A conductive carbon coat of ca. 10 nm was applied before SEM analysis.

3. Results:

3.1 EDX analysis:

EDX analysis was performed to confirm the compositions of the different glass formulations prepared in comparison with expected formulations (see Table 2). All the compositions were found to be close to the expected compositions (within a 2 % error margin). Figure 1 represents the 8 mol% and 10 mol% Y_2O_3 containing glass sample where 8 mol% glass became crystalline and the glass did not melt for 10 mol% glass sample.

3.2 XRD analysis:

The X-ray diffraction spectra of the different glass compositions are presented in Figure 2. Absence of any sharp crystalline peaks suggested that the glasses as prepared were amorphous. A single broad halo shaped peak was observed between 20° to 40° diffraction angle for Y0, Y1, Y3 and Y5 formulations. Tetragonal yttrium phosphate (YPO_4) crystal peaks were observed for Y8 glass formulation.

3.3 Density and Molar volume analysis:

The density and molar volume for the multicomponent glasses are presented in Figure 3. The density of glass particles increased from 2.56 to 2.74 g/cm^3 with the incorporation of 0 to 5 mol% Y_2O_3 into the glass system. In contrast, the change observed in molar volume was from 37.65 cm^3 mol^{-1} to 38.1 cm^3 mol^{-1} for the same glasses across the compositional variation.

3.4 Thermal analysis:

Figure 4 shows the DSC scans obtained for 0 to 5 mol% yttrium containing phosphate glass system at different heating rates (i.e. 5°C/min^{-1}, 10°C/min^{-1}, 15°C/min^{-1} and 20°C/min^{-1}). The DSC traces exhibited clear endothermic and exothermic peaks at glass transition (T_g) and crystallisation (T_c) temperature, respectively. The onset crystallisation temperature (T_x) has been defined as temperature corresponding to the intersection of the two linear portions of the transition between glass transition and crystallisation temperature. The values of T_g, T_X, T_c and processing window (i.e. T_x-T_g) at different heating rates are summarised in Table 3. As can be seen in Table 3, the T_g at different heating rates was similar for the yttrium free phosphate glass (355°-361°C) whereas the T_g at different heating rates increased from 368°-376°C, 386°-399°C and 415°-429°C for the glasses investigated with increasing Y_2O_3 content.

The variation of shifts in T_x for the varying glass formulations at different heating rates are presented in Figure 5. The T_c at different heating rates increased from 471°C to 537°C for 5°C, 480°C to 552°C for 10°C, 485°C to 564°C for 15°C and 492°C to 571°C for 20°C, with increasing (0 to 5 mol%) Y_2O_3 content, respectively as shown in Figure 4. The values of T_x and T_c are listed in Table 3.

The processing window (T_x–T_g) was also evaluated for the different compositions investigated which is an indication of their thermal stability (47). From Figure 6, it was seen that the processing window values increased as the Y_2O_3 concentration increased to 3 mol% and further addition of Y_2O_3 to 5 mol% showed a slight reduction in the thermal stability. It was also observed that the values of processing window were seen to increase with increase of heating rates for each formulation.

To validate the results, the glass formulations were heat-treated at two different temperature regimes; a) between 24-50°C above T_g to avoid crystallisation and explore any physical changes in their properties and b) between T_x and T_c to deliberately crystallise the samples and observe the crystal morphology formed.

"From Figures 7 (a-d), it was observed that needle shaped crystals had nucleated near to the glass surface. However, fewer needle shaped crystals were observed on the glass surface for the 5 mol % Y_2O_3 samples as seen in Fig. 7 (d)."

A heat treatment process (between T_x and T_c) at a heating rate of 10°C/min was applied to the different glass formulations investigated to explore the growth and morphology of the crystals observed. However, it was also observed that the needle like crystalline morphologies formed decreased in width with the addition of yttrium oxide.

3.6 Activation energies:

The activation energies for the T_g, T_x, T_c and overall crystallisation (E) region of the glasses were determined by utilising the equations outlined in supplementary section S1.

Activation energy of glass transition temperature:

The glass transition activation energies (E_g) obtained using equation 3 in supplementary section S1 are represented in Figure 9 and highlight the plots of lnα versus $1000/T_g$. The E_g values obtained from the slope of the straight lines are also highlighted in Figure 9. As can be seen, the E_g obtained using the Moynihan equation decreased from 191.82 to 118.12 KJ/mol with increasing Y_2O_3 from 0 to 5 mol%.

The E_g can also be determined utilising the Kissinger equation (see equation 4 in S1). A plot of ln (α/T_g^2) versus $(1000/T_g)$ is depicted in Figure 9. The activation energies here were also

observed to decrease from 183.68 to 113.40 KJ/mol with increasing Y_2O_3 content (0 to 5 mol%). The E_g values obtained from Kissinger equation were very similar to those obtained by Moynihan equation.

Onset crystallisation temperature activation energy:

The values of the onset crystallisation activation energy (E_x) were obtained using the Ozawa equation (see equation 5) based on the slope of $\ln\alpha$ vs $1000/T_x$ as shown in Figure 10. The values of E_x decreased from 189.74 to 118.27 KJ/mol with the incorporation of Y_2O_3 into the glass system.

The onset of crystallisation activation energies using Augis and Bennett method was also determined (based on equation 6 in S1). The E_x of the glasses estimated from plots of $\ln(\alpha/T_x)$ versus $1000/T_x$ are shown in Figure 10. The values of E_x were seen to decrease from 184.26 to 114.88KJ/mol with the incorporation of Y_2O_3 in the glass system.

Peak crystallisation activation energy:

The activation energy of crystallisation peak temperature (E_c) was also explored based on the Kissinger equation (see equation 7 in S1). The plot of $\ln(\alpha/T_c^2)$ versus $1000/T_c$ for the samples explored are shown in Figure 11. The value of E_c was calculated from the slope of each curve. It was clear from Figure 10 that the activation energy of crystallisation (E_c) decreased from 120.34 to 94.27 KJ/mol with increasing Y_2O_3 content.

Overall crystallisation activation energy:

The overall non-isothermal crystallisation activation energy (E) was calculated using the Matusita-Sakka equation, which represents the volume fraction of crystals (X) precipitating in a glass heated at a constant rate (α). From equation 8, the nucleation parameter (n) was determined by plotting $\ln[-\ln(1-X)]$ versus $\ln\alpha$ for three selected temperatures (within the

crystallisation peaks of the DSC traces obtained at each of the heating rates explored) as shown in Figure 12. The slope of the straight lines provided the value of nucleation and growth parameters (n) and the corresponding values are listed in Table 4. The nucleation parameters or Avrami exponent (n) were almost similar for the glass formulations tested. The dimensionality of crystal growth (m) depends on the Avrami exponent (n) and usually the dimensionality of crystal growth m is equal to n-1 (23). As such, a one-dimensional crystal growth was suggested based on the Avrami exponent values obtained for the glasses investigated (see Table 4).

With the order parameter n, m and plots of ln [-ln(1-X)] versus 1000/T at different heating rates, the overall crystallisation activation energy (E) of the glass formulations was estimated from Equation 9. These plots are presented in Figure 13. Overall the crystallisation activation energy decreased from 253.46 to 205.52 KJ/mol with the incorporation of Y_2O_3 in the glass system (see Table 4).

4. Discussion:

Yttrium containing phosphate-based glasses (PBGs) could be promising materials for biomedical applications such as radioembolisation therapy (48). However, from the glass formulations investigated, compositions above 5 mol% yttrium oxide content showed strong tendency towards crystallisation. The crystallisation kinetics and activation energy can provide a better understanding about the glass formability and thermal stability of glasses. In this study, the effect of Y_2O_3 incorporation into PBGs (upto 5 mol%) on crystallisation kinetics was investigated. Glasses containing more than 5 mol% yttrium oxide content (in this series) were not considered for analysis as these formulations rapidly crystallised (see Figure 1) and confirmed *via* XRD as shown in Figure 2.

Compositional analysis was confirmed *via* EDX and revealed that the respective oxide contents for the glasses investigated were within 2 mol% of their predicted values (see Table 2). The reduction of small amount of P_2O_5 content was observed and this was attributed to the effect of its volatilisation (49).

In general, for PBGs the density and molar volume are usually inversely related (50). However, in the present study for the glasses investigated, the density and molar volume increased with increasing yttrium oxide from 0-5 mol% (see Figure 3). Shaharuddin *et al.* reported that the density of phosphate glass was dependent on the atomic weight of the components added as well as compactness of the glass structure (51). The increase in density was attributed to the replacement of lower molar mass (61.97 g/mol) and density (2.27 g/cm^3) of Na_2O with higher molar mass (225.81 g/mol) and density (5.01 g/cm^3) of Y_2O_3 (11,14). Ebrahim *et al.* also found an increase in density (from 2.78 - 3.01 g/cm^3) for calcium magnesium aluminosilicate glass due to the addition of Y_2O_3 (from 0 to 3 mol%) in place of Al_2O_3 (22). Structural NMR analysis

on phosphate based glasses were studied by different authors in the literature (52–54) and reported that Q^1 and Q^2 structures were found for compositions with fixed P_2O_5 at 45 mol%. Fu *et al.* investigated the structural analysis on yttrium containing phosphate based glasses and they reported that yttrium acts as a network modifier (7). Mitang *et al.* stated that generally rare earth oxides acts as a network modifiers in the glass structure and the introduction of the modifier oxide into the glass structure breaks the glass network, which subsequently creates a Non Bridging Oxygen (NBO) (23). The increase of molar volume with increasing Y_2O_3 content was attributed to the increase in number of non-bridging oxygens which decreased the compactness of the glass structure subsequently leading to increase in molar volume. This increase in molar volume could also be attributed to the larger atomic radii of Y (240 pm) and bond length of Y-O (2.2 A°)(7) compared to the smaller atomic radii of Na (227 pm) and bond length of Na-O (2.051 A°) (55). Mi *et al.* studied the incorporation of Y_2O_3 in soda lime silicate glass and reported that the molar volume increased from 24.03 to 24.15 cm^3/mol with increasing Y_2O_3 content from 0 to 1 mol% due to an increase in the number of non-bridging oxygens, which subsequently decreased the compactness of the glass structure (56).

The thermal profiles of PBG are strongly dependent on their structure and composition (50). A gradual increase in glass transition temperature (T_g) for glass particles were observed with increasing yttrium oxide (from 0 to 5 mol%) content and with different heating rates (5°, 10°, 15° and 20°C / min) as shown in Figure 4. The T_g increased by ~60°C for 5°C and 10°C heating rate, ~65°C for 15°C heating rate and ~68°C for 20°C heating rate for 0, 1, 3 and 5 mol% Y_2O_3 respectively. This increase in T_g was attributed to the fact that the Y-O bond strength is greater than that of the Na-O bond as Y-O has greater bond dissociation energy (715 KJ/mol) compared to Na-O (257 KJ/mol). Constantini *et al.* investigated the thermal properties of

calcium yttrium silicate glass and found that the T_g value increased from 810° to 840°C with the incorporation of Y_2O_3 in place of CaO (from 0 to 0.33 mol%). They reported that this was due to replacement of the lower field strength of Ca^{2+} (2.04 $Å^{-2}$) and lower bond (Ca-O) strength (130 KJ/mol) with higher field strength of Y^{3+} (3.76 $Å^{-2}$) and greater single bond (Y-O) strength in the oxide structure (210 KJ/mol) (57,58).

In this study, the T_g values were also found to increase with increasing heating rates (see Table 3). This was attributed due to the decrease of structural relaxation which subsequently increase the glass transition temperature with increasing heating rates. Benson *et al*. stated that structural relaxation time of lithium phosphate glasses decreased with higher heating rates and was inversely proportional to the glass transition temperature (31). A similar study conducted by Kawamoto *et al.* found that the T_g decreased with the addition of MoO_3 into a ternary sodium borosilicate glass formulation (59). They reported that the decrease in T_g was due to the lowering of the viscosities and the increase of driving force with MoO_3 addition (59).

The onset crystallisation (T_X) and crystallisation peak (T_c) temperatures of the glass particles were also seen to increase with incorporation of yttrium oxide at different heating rates (see Table 3). The shift of T_x and T_c to higher temperature with different heating rate may be attributed to the easier relaxation of randomly arranged structures at slower heating rates where relaxation time is inversely proportional to the heating rate. Kasyap *et al.* studied the heating rate dependence of crystallisation temperature on Cu-Based metallic glass and found that metallic glass starts crystallising at lower temperatures as the structural relaxation happens more easily at slow heating rates (60). They also suggested that heating rate is inversely proportional to relaxation time and proportional to T_x and T_c (60). With increasing heating rates, the shift of T_c to higher temperature was observed which is mainly attributed

to the induction time associated with the nucleation process and crystallisation is controlled by nucleation. Khan *et al.* studied chalcogenide glasses and stated that T_c increased from 397°C to 440°C with increasing heating rate from 5 K to 25 K/min (61). They also mentioned that as the heating rate increases, the temperature at which induction time becomes zero increases leading to shift of T_C to higher temperatures. In addition, the T_c also increased with increasing Y_2O_3 content and this was ascribed to the heat flow of the samples increasing with increasing heating rate (62,63). Al-noaman *et al.* investigated the effect of MgO on bioactive glasses and reported that the T_c increased from 880°C to 920°C with increasing heating rates from 5°C to 20°C/min (64). Similar results were also found by Clupper and Hench (65) and Bretcanu *et al*. (66).

The thermal stability of the glass particles in terms of their processing window increased with the addition of yttrium oxide up to 3 mol% (see Table 3). This was suggested to be due to the replacement of P-O-P bonds (bond energy, 680 KJ/mol) by Y-O-P bonds which have a higher bond energy (1054 KJ/mol) (67). As a result, the cohesive energy increased with increasing Y_2O_3 content which increased thermal stability. However, further addition of Y_2O_3 decreased the thermal stability and this could be attributed due to the formation of quasicrystal which in turn decreases the glass forming ability (68). Zhuohao *et al.* studied Y_2O_3 doped germanate oxyfluoride glass ceramics and reported that their thermal stability decreased when yttrium content increased from 0 to 9.30 mol% due to their tendency to crystallise (69). Mehta *et al.* studied thermal stability of Se-Sb glassy alloys and reported an increase up to 4 mol% Sb content which decreased for 6, 8 and 10 mol % additions due to the decrease of bond energies (70). Similar results were also reported by Abhay *et al.* chalcogenide glass system (71) Furthermore, a lower atomic radius of yttrium (0.1801 nm) compared to sodium (0.1857 nm)

could have formed more dense atomic packing and consequently, improve thermal stability of the lower Y_2O_3 doped glasses (72).

Differential scanning calorimetry (DSC) has been widely used for investigating the crystallisation kinetics of glasses. Activation energy and crystallisation kinetics are important parameters and can be obtained using the equations proposed from the interpretation of non-isothermal data. For the different methods of analysis applied for the determination of activation energies of T_g, T_x and T_c for the four different glass formulations investigated, see supplementary section S1.

Moynihan and Kissinger equations were used for the determination of activation energy at glass transition temperature (E_g). Although the Moynihan and Kissinger equations are based on different theoretical models, the values of E_g were close to each other and the differences in values were within the experimental errors (see Figure 9). The E_g value decreased from 191 to 118 KJ/mol (via Moynihan method) and from 183 to 113 KJ/mol (via Kissinger method) with increasing Y_2O_3 content from 0 to 5 mol% (see Figure 9). E_g is directly related with the relaxation energy of glass structure. The relaxation energy is the amount of energy needed to overcome the barrier between different quasi-stable regions during the preparation of glass. Mitang *et al.* studied yttrium oxide containing silicate glass and reported that E_g was linked with to the structural relaxation energy and as such, E_g was inversely proportional to the stability of the glass structure (23). In addition, they stated that Y_2O_3 acts as a network modifier and its introduction into the glass structural network creates non-bridging oxygen's (NBOs), which can increase the disorder and entropy of the glass structure. Three types of activation energy can be involved in the crystallisation process, including activation energy for onset of crystallisation (E_X), for peak crystallisation (E_c) and for the overall crystallization (E). The E_x decreased from 189.74 to 118.27 KJ/mol (using Ozawa model) and

from 184.26 to 114.88 KJ/mol (using Augis-Bennette model) with increasing yttrium oxide content from 0-5 mol% (see Figures 10). Moreover, E_c decreased (from 120.34 to 94.27 KJ/mol) with increasing Y_2O_3 content via Kissinger method (see Figure 11). The reduction of E_x or E_c could be attributed to an increase in the number of non-bridging oxygens by the addition of Y_2O_3 acting as a network modifier (7,73). Therefore, the movement of atoms in glass structure was easier for the formation of crystal nucleation and growth. Zarabad *et al.* studied addition of Y_2O_3 on crystallisation kinetics of oxyfluoride glass ceramics and found the opposite results where the activation energy of crystallisation increased with incorporation of Y_2O_3 (74). They reported that Y_2O_3 acted as a network former and consequently, the formation of bridging oxygens which makes the movements of atoms difficult for crystallisation and as a result, an increase in the activation energy of crystallisation was observed.

The theory of transformation of crystallisation kinetics was developed by Johnson and Mehl (75) and Avrami (76). Matusita *et al.* developed a method of crystallization based on nucleation and growth processes (46,77). Crystallisation mechanisms such as bulk or surface crystallisation should be considered when investigating the activation energy. The Avrami exponent (n) can be used to understand the crystallisation process in glassy materials. The value of the dimensionality of growth (m) is related to the nucleation parameter/Avrami exponent (n) value. Usually, the dimensionality of crystal growth (m) is reported to be equal to n-1 (23). When surface crystallisation predominates; the value of the nucleation and growth parameters are equal to 1 (40). In our study, the nucleation or Avrami parameter (n) was found to be approximately 2 for all the glass formulations investigated (see Table 4). This suggested that one-dimensional crystal growth was occurring for the glasses investigated, which could be explained by the small addition of yttrium oxide in the glass system (78). SEM

analysis confirmed that the crystalline morphologies observed resembled one-dimensional structures in the form of needle like arrays, for all glass formulations investigated (as shown in Figure 8 (a-d). Mitang *et al.* studied yttrium doped zinc borosilicate glasses and found that one-dimensional crystal growth formed from the surface to the inside of the glass structure (23). From Figure 12d, deviations from the straight lines for Y5 glass formulation was observed at high temperature (550°C, 554°C and 558°C) which could be attributed to the saturation of nucleation sites during the latter stages of the crystallisation process (79). In addition, restriction of crystal growth by small size particles may also be responsible for the deviations observed at high temperature (80). The overall crystallisation activation energy (E) also decreased from 253 to 205 KJ/mol with increasing yttrium oxide content. Similar trends were also observed for other T_g, T_x and T_C activation energy values. The decrease of overall activation energy could also be attributed to the network modifying effect of Y_2O_3 forming NBOs.

In general, the E_g was higher than E_c due to the molecular motion around the T_g (81). A similar behaviour was noted for lithium ions in bismuthate glasses (82). In this study higher E_x value was found compared to E_c (see Figures 10 and 11) and this was attributed to the effect of bulk nucleation and crystal growth processes. Huan *et al.* also found higher E_x value compared to E_c for amorphous Zr-Cu-Ni alloys and suggested that the nucleation process of amorphous $Zr_{70}Cu_{20}Ni_{10}$ alloy was more difficult than the growth process (41).

In summary, the incorporation of Y_2O_3 into the glass system investigated decreased E_g, E_X and E_C and increased their thermal stability. Differences of activation energy values using Moynihan, Ozawa, Augis and Bennette, Kissinger and Matusita-Sakka plots were observed and attributed to the different temperatures involved in the various equations. The reduction in activation energy with incorporation of Y_2O_3 into the glass system implied that Y_2O_3 acted

as a nucleating agent promoting crystallisation effects. On the basis of activation energy values for this glass family series (with fixed 45 mol% P_2O_5), it could be suggested that yttrium containing PBGs with more than 5 mol% Y_2O_3 would crystallise as the activation energy reduced to lower than 200 KJ/mol.

5. Conclusions:

In this study, crystallisation kinetic studies were carried out for $45P_2O_5$-(30-x) Na_2O-25CaO - xY_2O_3 glass system using non-isothermal DSC measurements, which indicated that the glass transition and crystallisation temperatures were influenced by the heating rates. The activation energy of T_g, T_x and T_c was determined by five different methods. The T_g, T_X and T_C increased with the addition of Y_2O_3 into glass system while the E_g, E_x, E_c and E decreased. The Avrami parameter (n = 2), revealed the crystallisation kinetics to be controlled by bulk nucleation with one-dimensional growth predicted and observed via SEM analysis. It is suggested that Y_2O_3 acted as a nucleating agent in this glass family series and glasses with yttrium oxide content above 5 mol% would crystallise. The overall activation energy data also revealed that values close to or lower than 200 KJ/mol would very likely results in crystallisation of phosphate-based glasses in this family series.

Acknowledgements:

The authors would like to acknowledge the financial support provided by the University of Nottingham, Faculty of Engineering (Faculty of Engineering Research Excellence PhD Scholarship). The authors would also like to acknowledge the Nanoscale and Microscale Research Centre (nmRC) at the University of Nottingham for the support and help with SEM and FEG-SEM analyses.

References:

1. Bunker BC, Arnold GW, Wilder JA. Phosphate glass dissolution in aqueous solutions. J Non Cryst Solids. 1984;64(3):291–316.

2. Onyiriuka EC. Zinc phosphate glass surfaces studied by XPS. J Non Cryst Solids. 1993;163(3):268–73.

3. Brow RK, Tallant DR, Myers ST, Phifer CC. The short-range structure of zinc polyphosphate glass. J Non Cryst Solids. 1995;191(1–2):45–55.

4. Ahmed I, Collins CA, Lewis MP, Olsen I, Knowles JC. Processing, characterisation and biocompatibility of iron-phosphate glass fibres for tissue engineering. Biomaterials. 2004;25(16):3223–32.

5. Sharmin N, Rudd CD, Parsons AJ, Ahmed I. Structure, viscosity and fibre drawing properties of phosphate-based glasses: effect of boron and iron oxide addition. J Mater Sci. 2016;51(16):7523–35.

6. Martin RA, Salmon PS, Carroll DL, Smith ME, Hannon AC. Structure and thermal properties of yttrium alumino-phosphate glasses. J Phys Condens Matter. 2008;20(11):115204.

7. Fu Y, Christie JK. Atomic structure and dissolution properties of yttrium-containing phosphate glasses. Int J Appl Glas Sci. 2017;8(4):412–7.

8. Brow RK. Nature of alumina in phosphate glass: I, properties of sodium aluminophosphate glass. J Am Ceram Soc. 1993;76(4):913–8.

9. Donald IW, Metcalfe BL. Thermal properties and crystallization kinetics of a sodium

aluminophosphate based glass. J Non Cryst Solids. 2004;348:118–22.

10. Lakhkar NJ, Park J-H, Mordan NJ, Salih V, Wall IB, Kim H-W, et al. Titanium phosphate glass microspheres for bone tissue engineering. Acta Biomater. 2012;8(11):4181–90.

11. Neel EAA, Chrzanowski W, Knowles JC. Effect of increasing titanium dioxide content on bulk and surface properties of phosphate-based glasses. Acta Biomater. 2008;4(3):523–34.

12. Na YH, Kim NJ, Im SH, Cha JM, Ryu BK. Effect of Bi2O3 on structure and properties of zinc bismuth phosphate glass. J Ceram Soc Japan. 2009;117(1371):1273–6.

13. Sidek HAA, Hamezan M, Zaidan AW, Talib ZA, Kaida K. Optical characterization of lead-bismuth phosphate glasses. Am J Appl Sci. 2005;2(8):1266–9.

14. Singh S, Kalia G, Singh K. Effect of intermediate oxide (Y2O3) on thermal, structural and optical properties of lithium borosilicate glasses. J Mol Struct. 2015;1086:239–45.

15. Kokubo T, Kim H-M, Kawashita M, Nakamura T. Novel ceramics for biomedical applications. J Australas Ceram Soc. 2000;36(1):37–46.

16. Cacaina D, Ylänen H, Simon S, Hupa M. The behaviour of selected yttrium containing bioactive glass microspheres in simulated body environments. J Mater Sci Mater Med. 2008;19(3):1225–33.

17. Ghahramani MR, Garibov AA, Agayev TN. Production and quality control of radioactive yttrium microspheres for medical applications. Appl Radiat Isot. 2014;85:87–91.

18. Kawashita M, Matsui N, Li Z, Miyazaki T, Kanetaka H. Preparation, structure, and in

vitro chemical durability of yttrium phosphate microspheres for intra-arterial radiotherapy. J Biomed Mater Res Part B Appl Biomater. 2011;99(1):45–50.

19. Kawashita M, Matsui N, Li Z, Miyazaki T. Novel synthesis of yttrium phosphate microspheres for radioembolization of cancer. In: IOP Conference Series: Materials Science and Engineering. IOP Publishing; 2011. p. 192003.

20. Zhou H, Bhaduri SB. Preparation of Yttrium Phosphate and Yttrium-Doped Calcium Phosphate Microspheres via Hydrated Ions Exchange. Int J Appl Ceram Technol. 2015;12:E146–51.

21. Shakeri MS, Rezvani M. Optical band gap and spectroscopic study of lithium alumino silicate glass containing Y3+ ions. Spectrochim Acta Part A Mol Biomol Spectrosc. 2011;79(5):1920–5.

22. Mahdy EA, Ibrahim S. Influence of Y2O3 on the structure and properties of calcium magnesium aluminosilicate glasses. J Mol Struct. 2012;1027:81–6.

23. Wang M, Fang L, Li M, Li A, Zhang X, Hu Y, et al. Glass transition and crystallization of ZnO-B2O3-SiO2 glass doped with Y2O3. Ceram Int. 2019;45(4):4351–9.

24. Park J, Ozturk A. Effect of TiO2 addition on the crystallization and tribological properties of MgO–CaO–SiO2–P2O5–F glasses. Thermochim Acta. 2008;470(1–2):60–6.

25. Brauer DS, Karpukhina N, Law R V, Hill RG. Effect of TiO2 addition on structure, solubility and crystallisation of phosphate invert glasses for biomedical applications. J Non Cryst Solids. 2010;356(44–49):2626–33.

26. Kumar V, Pandey OP, Singh K. Thermal and crystallization kinetics of yttrium and

lanthanum calcium silicate glass sealants for solid oxide fuel cells. Int J Hydrogen Energy. 2011;36(22):14971–6.

27. Besson J-L, Lemercier H, Rouxel T, Trolliard G. Yttrium sialon glasses: nucleation and crystallization of Y35Si45Al20O83N17. J Non Cryst Solids. 1997;211(1–2):1–21.

28. Walck JC, Pantano CG. Sol gel processing and crystallization of yttrium aluminosilicates. J Non Cryst Solids. 1990;124(2–3):145–54.

29. Arita IH, Wilkinson DS, Purdy GR. Crystallization of yttria–alumina–silica glasses. J Am Ceram Soc. 1992;75(12):3315–20.

30. Wang M-T, Fang L, Li M. Effect of Rare Earth Dopant on Thermal Stability and Structure of ZnO-B~ 2O~ 3-SiO~ 2 Glass. J Inorg Mater. 2017;32(6):643–8.

31. Money BK, Hariharan K. Crystallization kinetics and phase transformation in superionic lithium metaphosphate (Li2O–P2O5) glass system. J Phys Condens Matter. 2009;21(11):115102.

32. Bae B, Weinberg MC. Crystallization of copper metaphosphate glass. J Am Ceram Soc. 1993;76(6):1395–400.

33. Koutsoukos P, Amjad Z, Tomson MB, Nancollas GH. Crystallization of calcium phosphates. A constant composition study. J Am Chem Soc. 1980;102(5):1553–7.

34. Zemenová P, Král R, Nitsch K, Knížek K, Cihlář A, Bystřický A. Characterization and crystallization kinetics of Er-doped Li 2 O–Y 2 O 3–P 2 O 5 glass studied by non-isothermal DSC analysis. J Therm Anal Calorim. 2016;125(3):1431–7.

35. Al-Ghamdi AA, Alvi MA, Khan SA. Non-isothermal crystallization kinetic study on

Ga15Se85− xAgx chalcogenide glasses by using differential scanning calorimetry. J Alloys Compd. 2011;509(5):2087–93.

36. Khan SA, Zulfequar M, Husain M. On the crystallization kinetics of amorphous Se80In20− xPbx. Solid State Commun. 2002;123(10):463–8.

37. Gao YQ, Wang W. On the activation energy of crystallization in metallic glasses. J Non Cryst Solids. 1986;81(1–2):129–34.

38. Deepika PK, Jain KS. Rathore, and NS Saxena. J Non-Cryst Solids. 2009;355:1274.

39. Cheng K. Determining crystallization kinetic parameters of Li2O–Al2O3–SiO2 glass from derivative differential thermal analysis curves. Mater Sci Eng B. 1999;60(3):194–9.

40. Erol M, Küçükbayrak S, Ersoy-Mericboyu A, Öveçoğlu ML. Crystallization behaviour of glasses produced from fly ash. J Eur Ceram Soc. 2001;21(16):2835–41.

41. Wang H-R, Gao Y-L, Ye Y-F, Min G-H, Chen Y, Teng X-Y. Crystallization kinetics of an amorphous Zr–Cu–Ni alloy: calculation of the activation energy. J Alloys Compd. 2003;353(1–2):200–6.

42. Vaish R, Varma KBR. The glass transition and crystallization kinetic studies on BaNaB9O15 glasses. J Phys D Appl Phys. 2008;42(1):15409.

43. Kissinger HE. Reaction kinetics in differential thermal analysis. Anal Chem. 1957;29(11):1702–6.

44. Ozawa T. Kinetic analysis of derivative curves in thermal analysis. J Therm Anal Calorim. 1970;2(3):301–24.

45. Singh AK, Mehta N, Singh K. Effect of indium additive on glass-forming ability and thermal stability of Se–Zn–Te chalcogenide glasses. Philos Mag Lett. 2010;90(3):201–8.

46. Matsushita K, Sakka S. Kinetic Study on Non-Isothermal Crystallization of Glass by Thermal Analysis (Commemoration Issue Dedicated to Professor Megumi Tashiro on the Occation of his Retirement). 1981;

47. Zhang W, Inoue A. Effects of Ti on the thermal stability and glass-forming ability of Ni-Nb glassy alloy. Mater Trans. 2002;43(9):2342–5.

48. Sene FF, Martinelli JR, Okuno E. Synthesis and characterization of phosphate glass microspheres for radiotherapy applications. J Non Cryst Solids. 2008;354(42–44):4887–93.

49. Ouchetto M, Elouadi B, Parke S. Volatilization from phosphate glass melts. Phys Chem Glas. 1991;32(5):202–6.

50. Sharmin N, Hasan MS, Parsons AJ, Furniss D, Scotchford CA, Ahmed I, et al. Effect of boron addition on the thermal, degradation, and cytocompatibility properties of phosphate-based glasses. Biomed Res Int. 2013;2013.

51. Shaharuddin SIS, Ahmed I, Furniss D, Parsons AJ, Rudd CD. Thermal properties, viscosities and densities of (50–x) Na2O–xCaO–50P2O5 glasses. Glas Technol J Glas Sci Technol Part A. 2012;53(6):245–51.

52. Ahmed I, Lewis M, Olsen I, Knowles JC. Phosphate glasses for tissue engineering: Part 1. Processing and characterisation of a ternary-based P2O5–CaO–Na2O glass system. Biomaterials. 2004;25(3):491–9.

53. Foroutan F. Sol-Gel Synthesis of Phosphate-Based Glasses for Biomedical Applications. UCL (University College London); 2015.

54. Kiani A, Lakhkar NJ, Salih V, Smith ME, Hanna J V, Newport RJ, et al. Titanium-containing bioactive phosphate glasses. Philos Trans R Soc A Math Phys Eng Sci. 2012;370(1963):1352–75.

55. Pavani PG, Suresh S, Mouli VC. Studies on boro cadmium tellurite glasses. Opt Mater (Amst). 2011;34(1):215–20.

56. Wang M, Cheng J, Li M, He F. Structure and properties of soda lime silicate glass doped with rare earth. Phys B Condens Matter. 2011;406(2):187–91.

57. Dimitrov V, Komatsu T. Average single bond strength and optical basicity of Na2O-GeO2 glasses. J Ceram Soc Japan. 2009;117(1370):1105–11.

58. Costantini A, Fresa R, Buri A, Branda F. Effect of the substitution of Y2O3 for CaO on the bioactivity of 2.5 CaO· 2SiO2 glass. Biomaterials. 1997;18(6):453–8.

59. Kawamoto Y, Clemens K, Tomozawa M. Effects of MoO3, on Phase Separation of Na2O-B2O3-SiO2 Glasses. J Am Ceram Soc. 1981;64(5):292–6.

60. Kasyap S, Prajapati S, Pratap A. Heating Rate and Composition Dependence of Crystallization Temperature of Cu-Based Metallic Glasses. In: Advanced Materials Research. Trans Tech Publ; 2016. p. 156–61.

61. Khan ZH, Khan SA, Alvi MA. Study of Glass Transition and Crystallization Behavior in Ga 15 Se 85-x Pb x (0⩽ x⩽ 6) Chalcogenide Glasses. Acta Phys Pol A. 2013;123(1).

62. Scott MG. The crystallization kinetics of Fe-Ni based metallic glasses. J Mater Sci.

1978;13(2):291–6.

63. Islam MT, Sharmin N, Rance GA, Titman JJ, Parsons AJ, Hossain KMZ, et al. The effect of MgO/TiO2 on structural and crystallization behavior of near invert phosphate-based glasses. J Biomed Mater Res Part B Appl Biomater. 2019;

64. Al-Noaman A, Rawlinson SCF, Hill RG. The role of MgO on thermal properties, structure and bioactivity of bioactive glass coating for dental implants. J Non Cryst Solids. 2012;358(22):3019–27.

65. Clupper DC, Hench LL. Crystallization kinetics of tape cast bioactive glass 45S5. J Non Cryst Solids. 2003;318(1–2):43–8.

66. Bretcanu O, Chatzistavrou X, Paraskevopoulos K, Conradt R, Thompson I, Boccaccini AR. Sintering and crystallisation of 45S5 Bioglass® powder. J Eur Ceram Soc. 2009;29(16):3299–306.

67. Luo Y-R. Comprehensive handbook of chemical bond energies. CRC press; 2007.

68. Dong W, Zhang H, Sun W, Ding B, Hu Z. Formation, thermal stability and mechanical properties of Zr-Nb-Cu-Ni-Al bulk metallic glasses. Mater Trans. 2006;47(5):1294–8.

69. Xiao Z, Luo M, Han R, Wang Y. Crystallization behaviour of Y2O3 doped germanate oxyfluoride glass-ceramics. Glas Technol J Glas Sci Technol Part A. 2015;56(4):126–31.

70. Mehta N, Tiwari RS, Kumar A. Glass forming ability and thermal stability of some Se–Sb glassy alloys. Mater Res Bull. 2006;41(9):1664–72.

71. Singh AK, Singh K. Crystallization kinetics and thermal stability of Se98-x Zn2In x chalcogenide glasses. Philos Mag. 2009;89(18):1457–72.

72. Luo J, Duan H, Ma C, Pang S, Zhang T. Effects of yttrium and erbium additions on glass-forming ability and mechanical properties of bulk glassy Zr–Al–Ni–Cu alloys. Mater Trans. 2006;47(2):450–3.

73. Jewell JM, Higby PL, Aggarwal ID. Properties of BaO–R2O3–Ga2O3–GeO2 (R= Y, Al, La, and Gd) Glasses. J Am Ceram Soc. 1994;77(3):697–700.

74. Zarabad MS, Rezvani M. Effects of Y2O3 on crystallization kinetics of SiO2-Al2O3-CaO-CaF2 oxy-fluoride glass-ceramic system. Results Phys. 2017;7:2958–64.

75. Marotta A, Saiello S, Branda F, Buri A. Activation energy for the crystallization of glass from DDTA curves. J Mater Sci. 1982;17(1):105–8.

76. Avrami M. Kinetics of phase change. I General theory. J Chem Phys. 1939;7(12):1103–12.

77. Matusita K, Komatsu T, Yokota R. Kinetics of non-isothermal crystallization process and activation energy for crystal growth in amorphous materials. J Mater Sci. 1984;19(1):291–6.

78. Samudrala K, Devarasetty SB. Investigation of Kinetics of crystallization Processes of S15-Se85, S15-Se81-Cu4 Chalcogenide glasses. In: IOP Conference Series: Materials Science and Engineering. IOP Publishing; 2016. p. 12176.

79. Heireche MM, Belhadji M, Hakiki NE. Non-isothermal crystallisation kinetics study on Se 90− x In 10 Sb x (x= 0, 1, 2, 4, 5) chalcogenide glasses. J Therm Anal Calorim. 2013;114(1):195–203.

80. Kaur G, Komatsu T. Crystallization behavior of bulk amorphous Se-Sb-In system. J Mater Sci. 2001;36(18):4531–3.

81. Paul T, Mountjoy G, Ghosh A. Thermal and structural investigations of xLi2O-(1− x) Bi2O3 (0.25≤ x≤ 0.35) glasses. Int J Appl Glas Sci. 2018;9(3):319–32.

82. Pan A, Ghosh A. Dynamics of lithium ions in bismuthate glasses. J Chem Phys. 2000;112(3):1503–9.

List of Tables:

List of Figures:

Figure 11: Plots of ln (α/T_c^2) versus $1000/T_c$ for $45P_2O_5$-(30-x) Na_2O-25CaO -xY_2O_3 (where x= 0, 1, 3 and 5) glass system

Figure 12: Plots of ln[-ln(1-X)] versus lnα at different temperatures for different compositions; (a) Y0, (b) Y1, (c) Y3 and (d) Y5

Figure 13: Matusita plots of ln [-ln(1-X)] versus 1000/T at different heating rates for $45P_2O_5$-(30-x) Na_2O-25CaO -xY_2O_3 (where x= 0, 1, 3 and 5) glass system

Supplementary Figure:

Figure S1: A schematic diagram of differential scanning calorimetry curve for the determination of crystallised volume fraction X at specific temperature T

Table 1: Glass codes, drying, melting and casting temperature used throughout the study

Glass Code	P_2O_5 content (mol%)	CaO content (mol%)	Na_2O content (mol%)	Y_2O_3 content (mol%)	Drying temp./time (°C/hr)	Melting temp./time (°C/hr)	Casting temp./time (°C/hr)
Y0	45	25	30	---	350/0.5	1150/2	374/1
Y1	45	25	29	1	500/1	1300/2	385/1
Y3	45	25	27	3	500/1	1300/2	406/1
Y5	45	25	25	5	500/1	1300/2	433/1

Table 2: Elemental composition for different phosphate-based glass formulations investigated using EDX analysis

Sample	P_2O_5 (Expected/Actual value) (mol%)	CaO (Expected/Actual value) (mol%)	Na_2O (Expected/Actual value) (mol%)	Y_2O_3 (Expected/Actual value) (mol%)
Y0	45 / 43.9±1.4	25 / 25.5±1.8	30 / 30.6±1.8	0 / 0
Y1	45 / 43.2±1.9	25 / 26.9±1.9	29 / 29.1±1.4	1 / 0.8±0.4
Y3	45 / 46.2±1.3	25 / 25.9±2.1	27 / 25.9±1.5	3 / 2±1.2
Y5	45 / 43.8±1.8	25 / 26.2±1.7	25 / 26.3±1.9	5 / 3.7±1.5
Y8	Glass became crystalline during cooling (see Figure 2)			
Y10	Glass did not melt at all (see Figure 1b)			

Table 3: Glass transition temperature T_g, onset crystallisation temperatures T_x, crystallisation temperature T_c and processing window of yttrium phosphate glasses

Sample	Heating rate (°C/min)	Glass transition T_g (°C) (±1)	Onset crystallisation T_x (°C) (±1)	Crystallisation temperature T_c (°C) (±1)	Processing window T_x-T_g (°C)
Y0	5	355	442	471	87
	10	356	446	480	90
	15	360	450	485	90
	20	361	454	492	93
Y1	5	368	462	495	94
	10	370	469	507	99
	15	375	473	513	98
	20	376	480	520	104
Y3	5	386	500	531	114
	10	391	515	549	124
	15	396	518	558	122
	20	399	523	564	124
Y5	5	415	520	537	105
	10	417	534	552	117
	15	425	540	564	115
	20	429	549	571	120

Table 4: Values of overall crystallisation activation energy, nucleation parameter (n) and dimension parameter (m) for $45P_2O_5$-(30-x) Na_2O-25CaO -xY_2O_3 (where x= 0, 1, 3 and 5) glass system

Sample	Overall crystallisation activation energy (KJ/mol)-Matusita-Sakka equation	Avrami index/Nucleation and growth parameter (n)	Dimensionality of growth (m)
Y0	253	2.0	1
Y1	216	2.1	1
Y3	211	2.2	1
Y5	205	2.1	1

List of Figures:

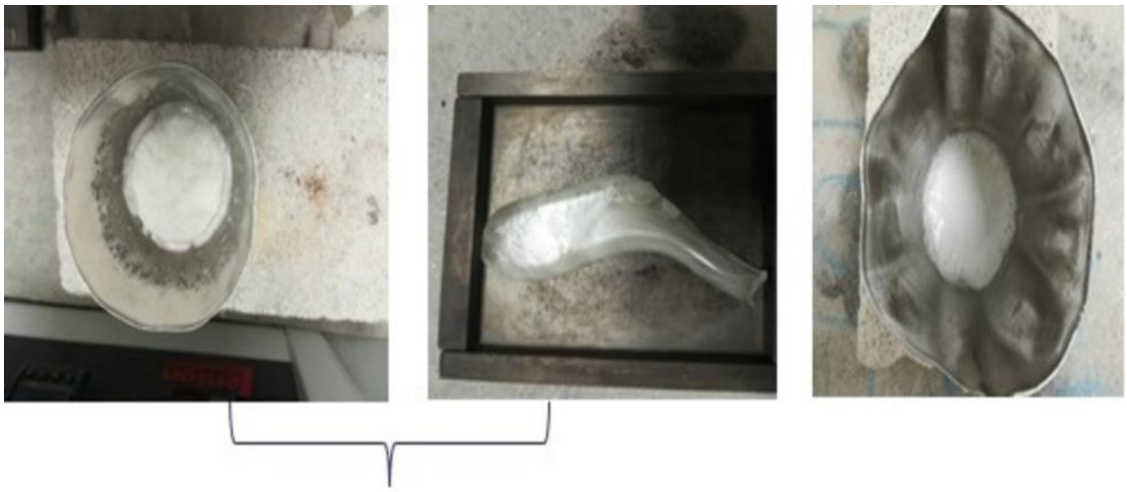

(a) **(b)**

Figure 1: Representative images of a) 8 mol% crystallised glass sample and b) 10 mol% sample for $45P_2O_5$-(30-x) Na_2O-25CaO -xY_2O_3 (x= 8 and 10) glass system.

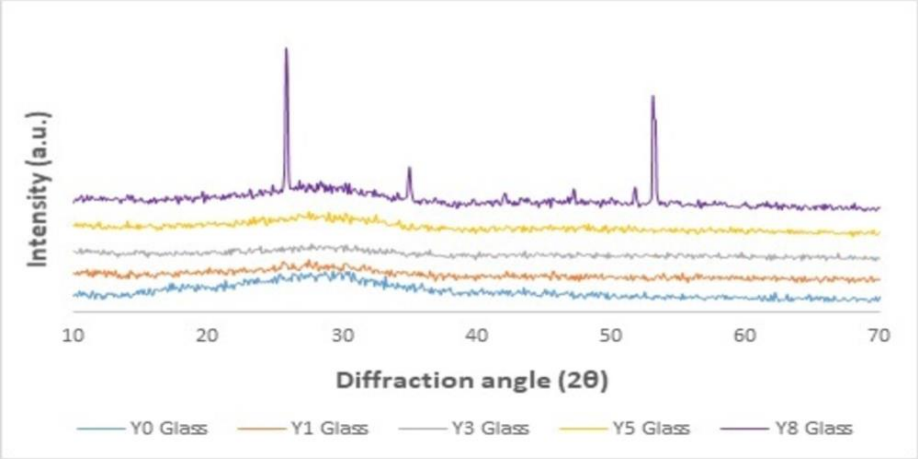

Figure 2: X-ray diffraction pattern for glasses in the system of $45P_2O_5$-(30-x) Na_2O-25CaO - xY_2O_3 (where x= 0, 1, 3, 5 and 8)

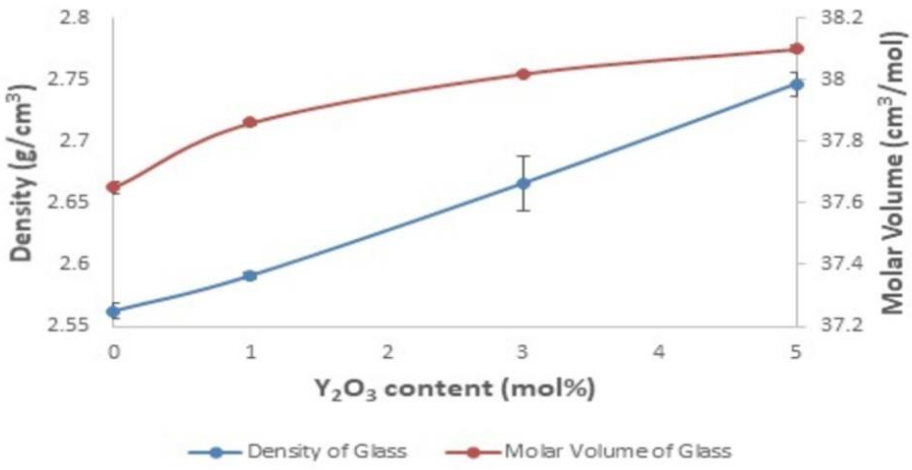

Figure 3: Density and Molar volume of phosphate glass particles as a function of Y_2O_3 content; error bars represent standard error of mean where n = 3.

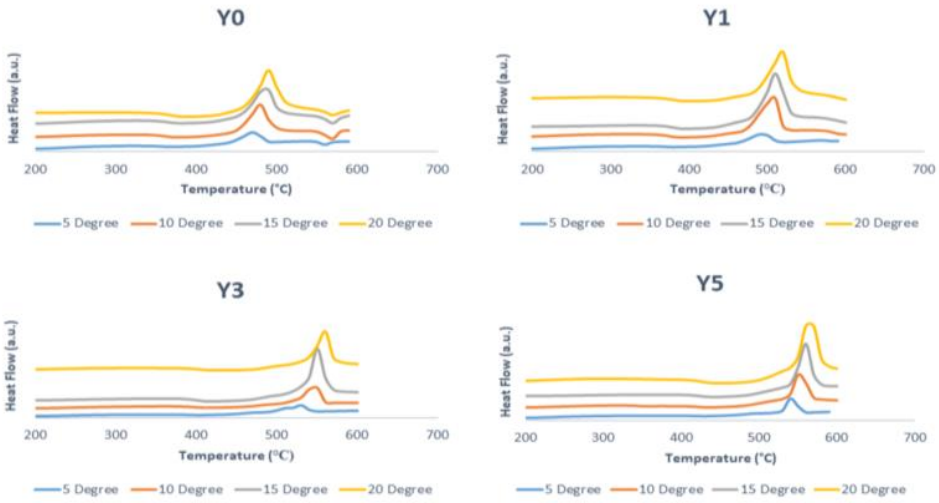

Figure 4: DSC traces for glass particles investigated in the glass system $45P_2O_5$-(30-x) Na_2O-25CaO-xY_2O_3 (where x=0, 1, 3 and 5) at different heating rates (5°C, 10°C, 15°C and 20°C/min^{-1})

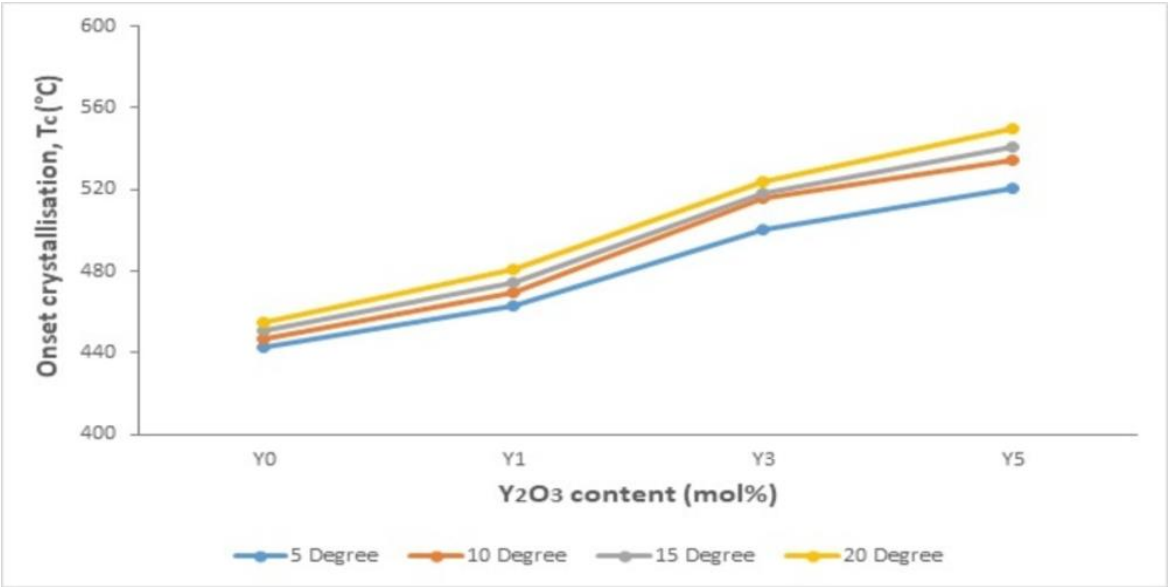

Figure 5: Variation of onset crystallisation temperature (T_x) with Y_2O_3 content at different heating rates

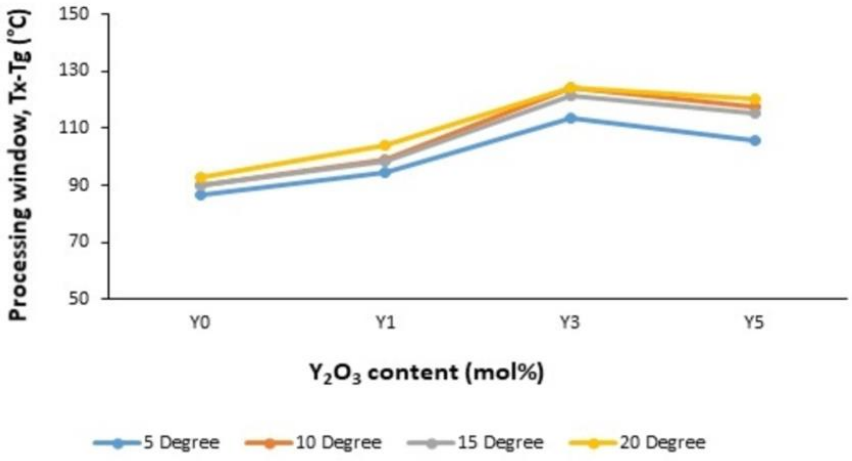

Figure 6: Variation of processing window (T_x-T_g) with Y_2O_3 content at different heating rates

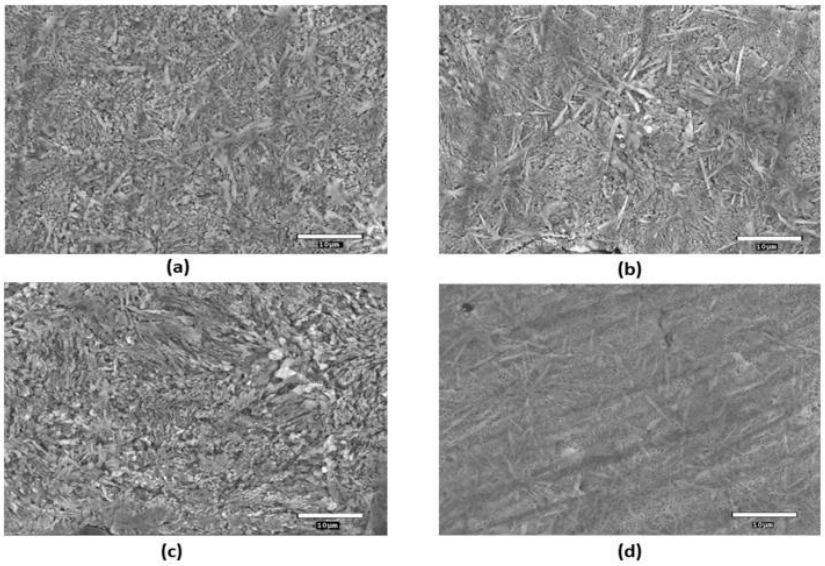

Figure 7: SEM micrographs of surface microstructure in glass samples-(a) Y0 and (b) Y1 heat treated at 406°C for 5h, (c) Y3 and (d) Y5 heat treated at 441°C for 5h

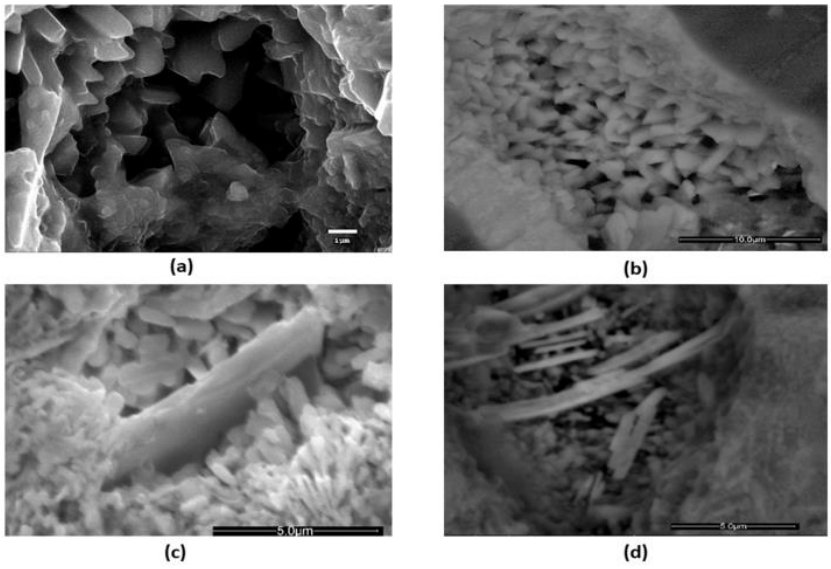

Figure 8: SEM micrographs exploring crystal growth formation for-(a) Y0 and (b) Y1 heat treated at 476°C for 5h, (c) Y3 heated at 535°C and (d) Y5 heat treated at 545°C for 5h

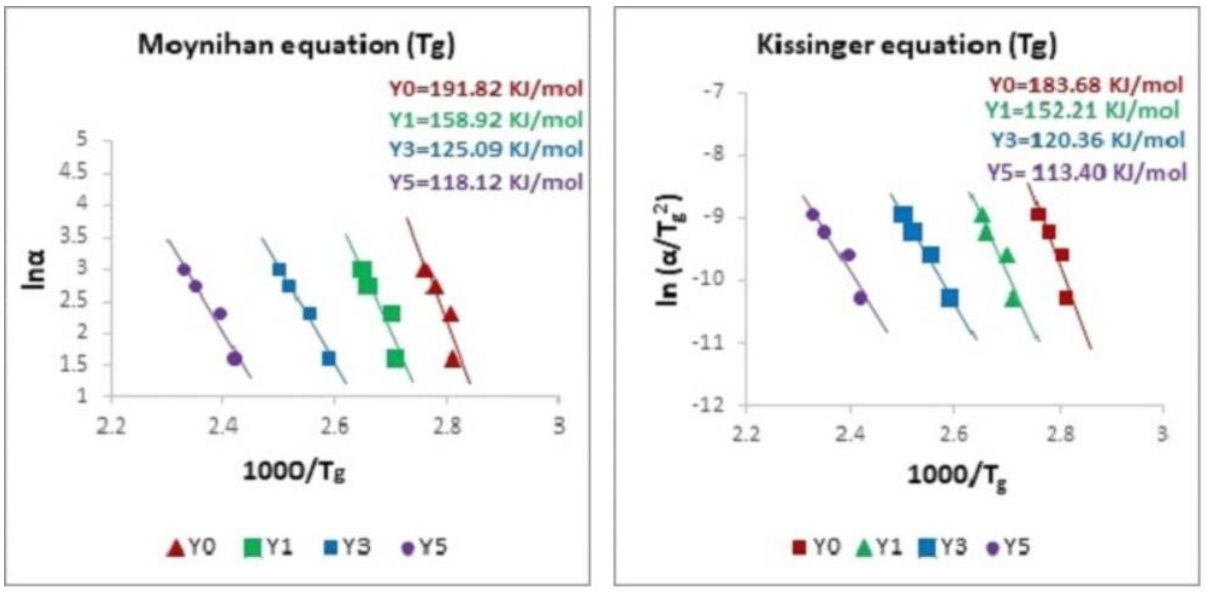

(a) (b)

Figure 9: Plots of a) lnα versus 1000/T_g and b) ln (α/T_g^2) versus 1000/T_g for 45P_2O_5-(30-x) Na_2O-25CaO -xY_2O_3 (where x= 0, 1, 3 and 5) glass system

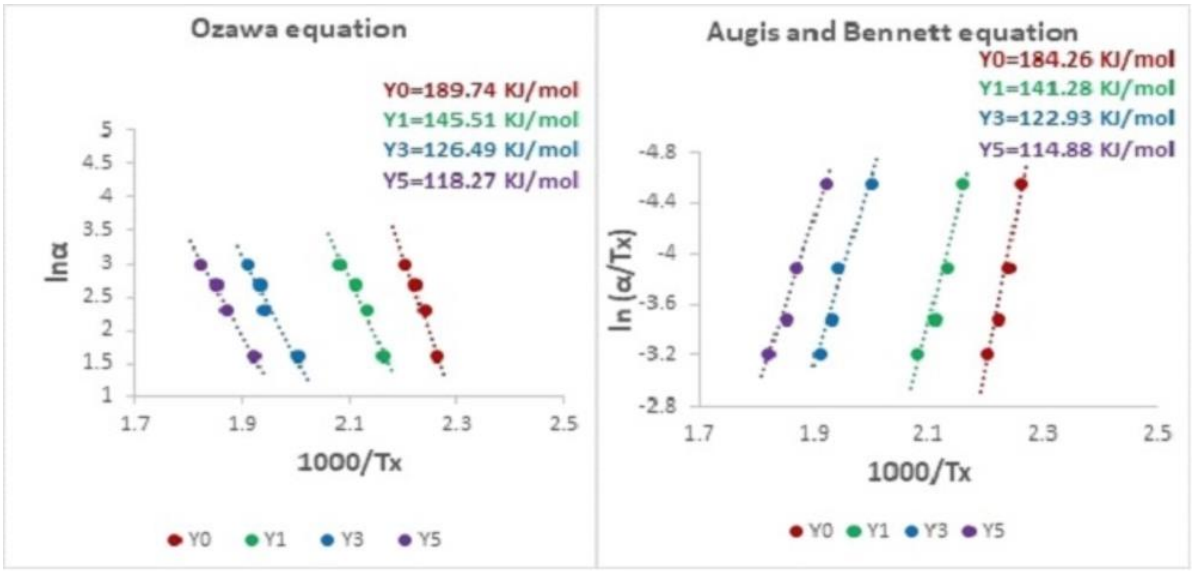

(a) (b)

Figure 10: Plot of a) lnα as a function of 1000/T_x and b) ln (α/Tx) as a function of 1000/Tx for 45P_2O_5-(30-x) Na_2O-25CaO -xY_2O_3 (where x= 0, 1, 3 and 5) glass system

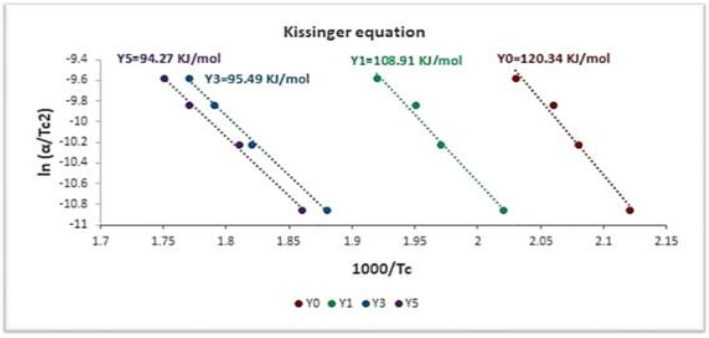

Figure 11: Plots of ln (α/T_c^2) versus $1000/T_c$ for $45P_2O_5$-(30-x) Na_2O-25CaO -xY_2O_3 (where x= 0, 1, 3 and 5) glass system

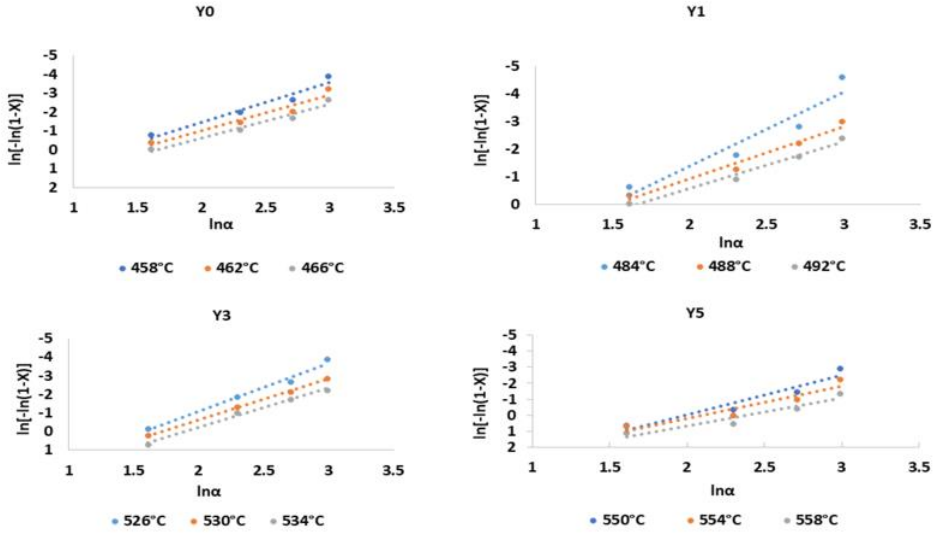

Figure 12: Plots of ln[-ln(1-X)] versus lnα at different temperatures for different compositions

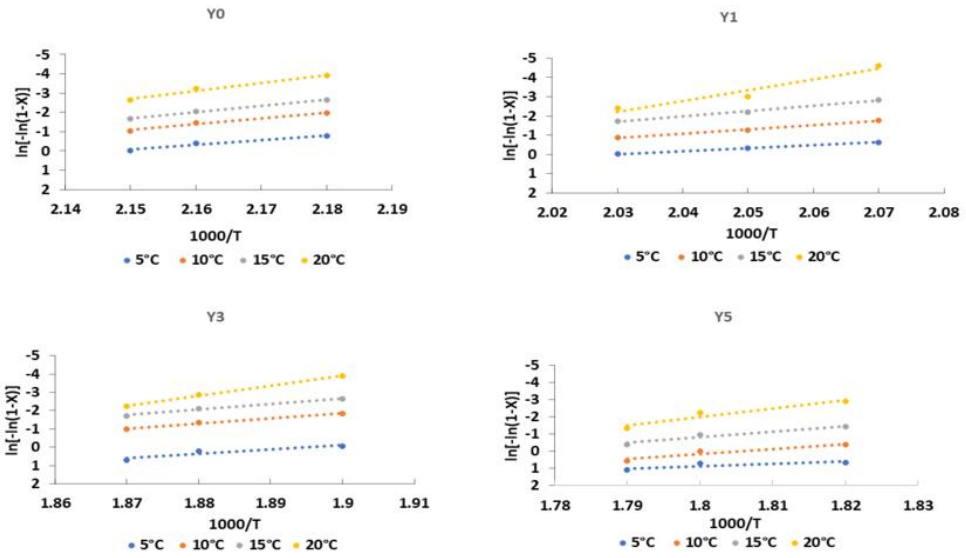

Figure 13: Matusita plots of ln [-ln(1-X)] versus 1000/T at different heating rates for $45P_2O_5$-(30-x) Na_2O-25CaO -xY_2O_3 (where x= 0, 1, 3 and 5) glass system

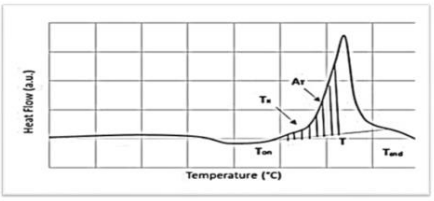

Figure S1: A schematic diagram of differential scanning calorimetry curve for the determination of crystallised volume fraction X at specific temperature T